Inertial Effects on Polymer Chain Scission in Planar Elongational Cross-Slot Flow

Mohammad T. Islam, Siva A. Vanapalli, and Michael J. Solomon*

Department of Chemical Engineering, University of Michigan, Ann Arbor, Michigan 48109

Received August 24, 2003; Revised Manuscript Received December 2, 2003

ABSTRACT: The molar mass and molar mass distribution of polymers subjected to chain scission in planar elongational flow are profoundly affected by the inertial character of the flow, as quantified by the Reynolds number. The degradation of dilute poly(ethylene oxide) (PEO) chains in aqueous-based solvents of varying viscosity was quantified in the planar elongational flow of a cross-slot flow device by gel permeation chromatography with multiangle laser light scattering detection. At low Reynolds number (Re < ∼1000), the steady-state weight-average molar mass, $M_{w,f}$, of the scission product distribution scaled with the nominal applied strain rate, $\dot{\epsilon}$, as $\dot{\epsilon} \propto M_{w,f}^{-1.93\pm0.15}$ for PEO/viscous solvent system and $\dot{\epsilon} \propto M_{w,f}^{-2.25\pm0.10}$ for the PEO/water system. At greater Reynolds number (Re > ∼1000), the observed scaling was $\dot{\epsilon} \propto M_{w,f}^{-1.04\pm0.07}$. Differences of this kind, first quantified by comparing results from stagnation point elongation flows and contraction flows, have previously been attributed to different molecular mechanisms of scission. Yet, our observations in different Reynolds number regimes suggest an alternative explanation based on fluid mechanics for the difference in steady-state scaling exponent. Measurements of pressure drop across the cross-slot flow support this alternative hypothesis.

I. Introduction

High molecular weight polymers in solution are susceptible to chain scission or degradation by flow-induced mechanical stress.[1−11] Elucidation of the interaction between the polymer molecule and the applied flow that results in scission is of fundamental interest because it involves a mechanism linking molecular (bond dissociation) and continuum (mechanical stress) processes.

Models of the scission of an isolated chain subjected to an idealized flow in a viscous solvent are available.[12−14] Above a critical rate of strain ($\dot{\epsilon}$), a polymer chain stretched due to the quasi-steady elongational flow in the vicinity of a stagnation point is predicted to rupture with high probability at its midpoint due to tension induced by viscous drag.[1] In this case, for initially monodisperse chains, $\dot{\epsilon}_f \sim M^{-2}$. Here $\dot{\epsilon}_f$ is the critical strain rate for scission in the stagnation point flow, and M is the molar mass of the polymer sample. In the fast transient flow mechanism for scission, polymer chains experience a strong flow for only a short residence time ($<\tau$, the characteristic relaxation time of polymer chains), and scission occurs while the individual chains are partially stretched.[2] Flow through an abrupt or tapered contraction has been used as a model of fast transient flows.[2] The fast transient flow mechanism yields $\dot{\epsilon}_f \sim M^{-1}$.[2,14] The agreement between these theories and the experimental literature is good: $\dot{\epsilon}_f \sim M^{-2}$ has been quantified in stagnation point flows,[1] while $\dot{\epsilon}_f \sim M^{-1}$ has been observed in contraction flow.[2,15] Moreover, in many cases scission has been reported to occur predominantly at the midpoint.[1,2,4,16,17]

Thus, simple theoretical models of flow-induced chain scission are apparently corroborated by available experimental data. Yet, unresolved issues remain, and additional experimental study of scission in dilute polymer solutions is warranted for the following four reasons:

First, literature reports that the chain scission exponents of −2 and −1 for quasi-steady elongational flow and fast transient flow, respectively, were characterized in experiments over a broad range of the Reynolds number with some experiments occurring at Reynolds number as high as 10 000.[2] The role of flow field modification due to inertial effects and its subsequent effect on polymer chain scission should be more thoroughly explored.

Second, the literature distinguishes between the mechanism of scission in quasi-steady stagnation point flows and in fast transient flows like flow through an abrupt contraction.[9] Yet, experimentally, high strain rate quasi-steady stagnation point flows are typically generated in devices with small (<1 mm) characteristic dimensions.[3,18] These small dimensions are often achieved by means of an abrupt contraction upstream of the quasi-steady stagnation point flow. The interaction between these two flows and its possible effect on chain scission product distributions has yet to be assessed.

Third, in stagnation point elongational flow, chains traversing the flow break with low probability because they must experience strain sufficient to generate the tension required for bond dissociation.[1] Thus, an ensemble of polymer chains must traverse the flow many times before most chains have passed through the high strain region in the vicinity of the stagnation point. Estimates of scission rate (on a per pass basis) from reported stagnation flow experiments vary widely: Values of 0.5%[19] and 0.1−10%[20] have been reported. The origin of this variation should be investigated.

Fourth, chain scission in both stagnation point elongational flows and fast transient flows is predicted to occur with high probability at the chain midpoint. Yet, recent Brownian dynamics simulations of polymer chains in elongational flows indicate that chains adopt an array of conformations, many of which are not symmetric about the midpoint.[21,22] Experiments,[1−4,17]

* Corresponding author: e-mail mjsolo@umich.edu, Tel (734) 764-3119, Fax (734) 763-0459.

10.1021/ma035254u CCC: $27.50
Published on Web 01/16/2004

Table 1. Molar Mass Distribution of PEO Samples

sample	M_w (g/mol)	M_w/M_n
PEO5M	$4.71\times 10^6 \pm 32000$	1.44
PEO920K	$9.34 \times 10^5 \pm 7700$	1.02
PEO200K	$2.22 \times 10^5 \pm 3200$	1.00

with a few exceptions,[5−7,22] tend to support the midpoint scission hypothesis. The relationship among scission theories, elongational flow simulations of polymer conformation, and chain scission experiments in various inertial flow regimes should be better reconciled.

In this paper we investigate the effect of Reynolds number on the polymer chain scission molar mass distribution by varying the solvent viscosity of solutions passed through the planar elongational flow of a cross-slot device. Thus, we address the first two unresolved issues described above. To study, for the first time, the effects of the contraction flow that is commonly upstream of any cross-slot stagnation point flow, we measure the scission molar mass distribution in two devices: one in which the contraction upstream of the stagnation point flow is abrupt, and the other in which it is gradual. This paper builds upon the pioneering work of Keller, Odell, and co-workers[1,3,10,20,23] and Kausch, Nguyen, and co-workers[2,7,9,24,25] by quantifying the profound role of inertial effects, quantified by the Reynolds number, on scission molar mass distribution products realized in cross-slot planar elongational flow.

II. Experimental Section

A. Materials. Dilute solutions of poly(ethylene oxide) (PEO) of varying molar mass distribution dissolved in aqueous-based solvents were studied. Aqueous based solutions were studied because of the requirement of significant volume of solution for flow experiments and because the viscosity of solution could be homologously varied by addition of glycerol. Poly(ethylene oxide) was selected for study because it is available in both polydisperse (Polysciences, Warrington, PA) and monodisperse (Polymer Laboratories, Amherst, MA; American Polymer Standards, Mentor, OH) quantities. Moments of the molar mass distribution of these materials, as characterized by gel permeation chromatography (GPC) and multiangle light scattering (cf. section II.C), are reported in Table 1. Solvents were deionized distilled (DDI) water and mixtures of DDI water and glycerol (Sigma-Aldrich): weight ratio 50/50, viscosity 6.4×10^{-3} Pa s.

To minimize shear, oxidative, and microbial degradation of PEO solutions, the following procedure was used to prepare test solutions: PEO stock solutions at concentration of 1000−2000 ppm were prepared in 0.1 M $NaNO_3$ buffer solutions of deionized distilled water so as to match GPC solvent conditions for its optimal performance (cf. section II.C). Before polymer dissolution, solvents were filtered through membranes with 0.2 μm pore size (Millipore, Bedford, MA). In addition, 1.0 wt % 2-propanol and 200 ppm hydrazine were added to prevent oxidative and microbial degradation, respectively.[26] To prevent shear degradation, PEO dissolution was performed in 1 L bottles rotated at 3−6 rpm (Wheaton Science Products, Millville, NJ). Dissolution required 1−3 days by this method. Before use, stock solutions were diluted to the desired polymer concentration by addition of filtered deionized distilled water and/or glycerol. To minimize the effect of other mechanisms of degradation, experiments were performed within 2−3 days after dilution to the desired concentration.

The solvent quality of the aqueous PEO solutions was assessed at $T = 22$ °C by extracting the scaling of the intrinsic viscosity, $[\eta]$, with molecular weight for monodisperse standards ($M_w = 29\,500-1.0 \times 10^6$ g/mol; $M_w/M_n < 1.1$) measured with an automated Ubbelohde capillary viscometer (Schott AVS-350, ViscoAlpha, Middletown, NY). The scaling relationship found, $[\eta] = 0.170M_w^{0.57}$, indicates that the aqueous solvent is marginal for PEO with excluded-volume exponent, $\nu = 0.52$.

B. Planar Elongational Cross-Slot Flow Apparatus. The central stagnation region in planar cross-slot flow is an approximation of planar elongational flow with nominal strain rate $\dot{\epsilon} = Q/d^2l$. Here Q is the volumetric flow rate, d is the slot dimension, and l is the slot depth.[18,27,28] Two possibilities for the generation of planar cross-slot flow are shown schematically in Figure 1a,c. Both schematics acknowledge the fact that in a high-strain rate flow fluid will typically be delivered to the cross-slot by means of a contraction to avoid high rates of deformation in the remainder of the flow loop. The contraction can affect chain scission directly, since contraction flow is a mixed flow with an elongational component or, indirectly, since molecules can be preconditioned in the contraction flow before they enter the central stagnation region of the cross-slot flow. We addressed the former issue by investigating two arrangements for delivery of the fluid to the cross-slot: (1) an abrupt contraction and (2) a tapered contraction. Comparison of the scission product distribution generated by the two flows will allow the role of the upstream contraction to be assessed. We addressed the latter issue by separating the contraction and the cross-slot by a distance that corresponds to approximately 3−30 Zimm relaxation times at the highest flow rate studied. Thus, molecules subjected to extensional deformation in the contraction are expected to have relaxed their conformations before entering the stagnation zone of the cross-slot device. However, it is unavoidable that molecules may be conformationally preconditioned by the shear flow in the channel prior to the cross slot region.[29] Details of the fabrication of the two flow devices are the following:

*Flow Cell 1 (FC-1): Upstream Abrupt Contraction***.** Flow cell 1 was constructed from four glass blocks (BK 7 optical glass) (Figure 1a). The slot dimension was 500 μm × 500 μm. The approach length to the slot was 10 mm to ensure fully developed flow at the cross-slot. The blocks were glued in place by two glass walls, which formed the boundaries in the neutral direction. To avoid possible end effects, the length in the neutral direction (1 cm) was much greater than the slot dimension. A 3D drawing of FC-1 is shown in Figure 1b. The four slots (500 μm × 10 mm) of FC-1 were connected to the external tubing of circular cross-section through four end fittings. O-rings were used to seal the interfaces between end fittings and the slots of the flow cell. At the interface where the end fittings met the slots, there was a step change in cross-section (area ratio ∼ 16:1).

Flow Cell 2 (FC-2): Upstream Tapered Contraction. Similar to FC-1, FC-2 was also constructed from four BK 7 glass blocks, and the slot dimension was 500 μm × 500 μm. Additionally, a 25.5 mm long trapezoidal section (at an approach angle of 7.5°) ahead of each of the four sides was provided to ensure gradual contraction from 7.16 mm × 7.16 mm area to 7.16 mm × 500 μm area (Figure 1c). The 7.16 mm dimension is the length in the neutral direction. After the tapered section, an approach length of 10 mm was used to ensure fully developed flow at the cross-slot. The four blocks were glued in place by two glass walls, which formed the boundaries in the neutral direction. The ends of the tapered sections (7.16 mm × 7.16 mm) were connected to the external tubing (i.d.: 7.16 mm) through aluminum blocks. Inside the blocks, the cross section was changed from circular to square by performing a gradual profile change over 12.7 mm length using electron discharge machining (EDM) (Figure 1d).

Flow Apparatus. Volumetric flow was delivered to the cross-slot flow devices through a pressure driven system shown schematically in Figure 2. To obtain steady flow, regulated, pressurized nitrogen gas was supplied to a 20 L reservoir from which PEO solutions were delivered to the flow conduit. Multipass experiments were accomplished by returning the solution from the collection tank to the supply reservoir. A pump driven flow apparatus was used for low volumetric flow rates. To prevent degradation inside the pump, polymer solutions were circulated through a peristaltic pump (Tat Pumps, model 41025Z, Logan, OH). A pulsation dampener

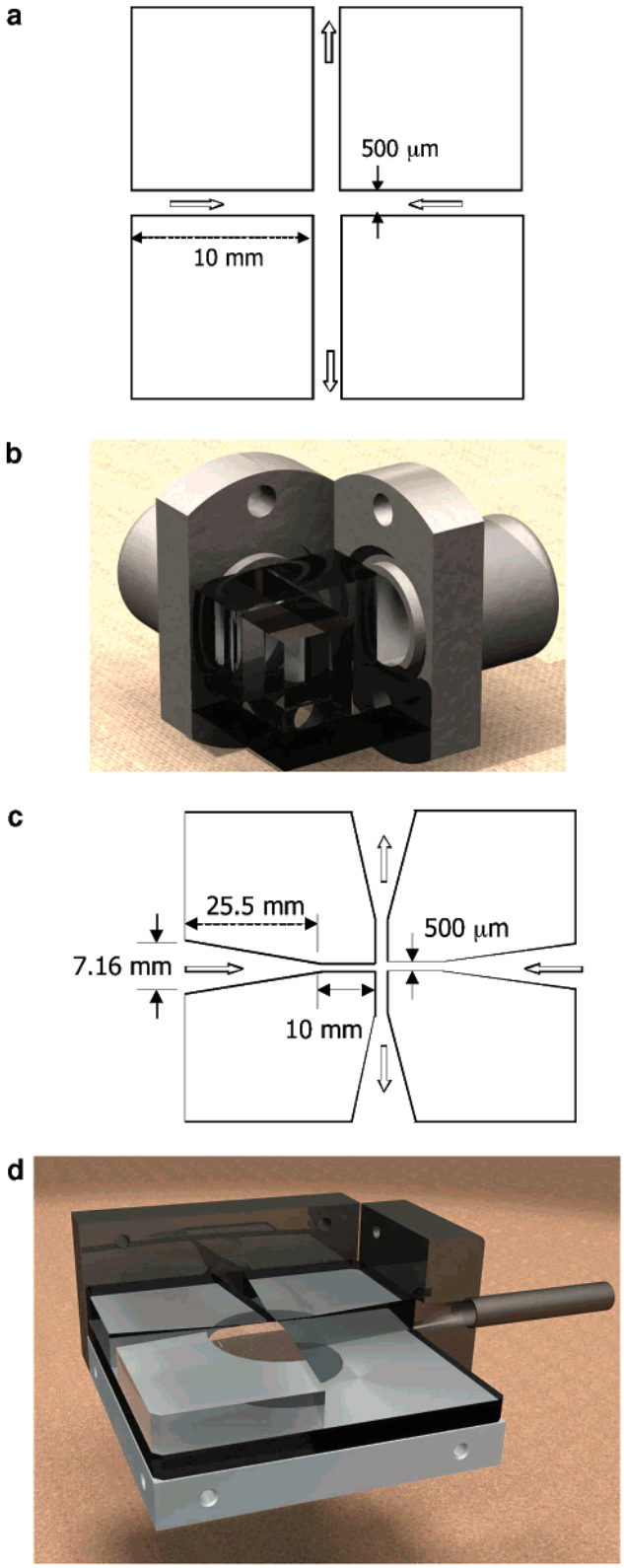

Figure 1. Diagrams of the flow cells: (a) flow cell with abrupt upstream contraction (FC-1), (b) 3-D view of FC-1, (c) flow cell with gradual upstream contraction (FC-2), (d) 3-D view of FC-2.

employed downstream of the pump and before the flow cell ensured uniform flow through the flow device.

Birefringence Characterization of Chain Deformation in Cross-Slot Flow. Prior flow-field characterization of stagnation flow devices has focused on characterization of chain orientation and stretching by means of birefringence.[1,14,30] To establish correspondence between our flow geometry and previous lit-

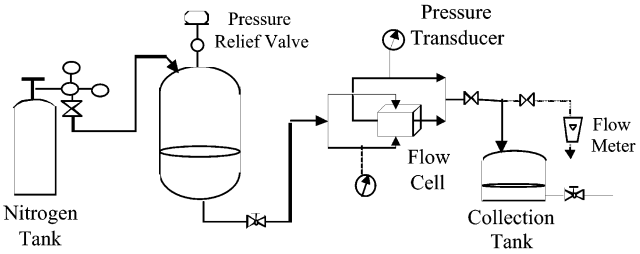

Figure 2. Schematic of the pressure driven flow apparatus used to perform scission experiments.

erature devices, we applied a phase-modulated polarization scheme described by Fuller.[18] The birefringence device used in the study consisted of a helium−neon laser (L), linear polarizer (LP), quarter-wave retarder (Q), photoelastic modulator (PEM) (Hinds Instruments, Hillsboro, OR), and a circular polarizer (CP) configured as follows: $LP_{@90°}PEM_{@45°}Q_{@0°}S_{\delta,@\chi°}CP$. All orientation angle subscripts are defined relative to the flow direction in the exit plane. Here S represents a polymer sample with birefringence retardation δ and orientation angle χ. In the PEM, the electric field along the slow axis (45° axis) is retarded relative to its value along the fast axis, which is perpendicular to the slow axis, by an amount δ_{PEM} that varies with time in a sinusoidal fashion [$\delta_{PEM} = \delta_{PEM,0} \sin(\Omega t)$]. A high-speed photodetector interfaced with two lock-in amplifiers and a low-pass filter was used to measure the time-dependent changes in optical intensity and recover information about flow-induced retardation (δ) of polymer samples.

The intensity and polarization of the light beam at the end of the optical train can be estimated by multiplying the Stokes vector of the incident light with the Muller matrices of the optical elements present between the detector and the laser source. By detecting one even and one odd harmonic (I_Ω and $I_{2\Omega}$) using lock-in amplifiers and normalizing them with the signal from the low pass filter (I_{dc}), two independent equations (independent of I_0) can be obtained.[31]

$$R_\Omega \equiv \frac{I_\Omega}{-I_{dc} \times 2J_1(\delta_{PEM,0})} = \cos(2\chi)\sin(\delta)$$

$$R_{2\Omega} \equiv \frac{I_{2\Omega}}{-I_{dc} \times 2J_2(\delta_{PEM,0})} = \sin(2\chi)\sin(\delta)$$

The above two equations can be solved to obtain flow-induced retardation, δ. Then the birefringence $\Delta n = (\lambda\delta)/(2\pi l)$, where λ is the wavelength of light and l is the path length in the neutral direction.

A condenser lens was used after the quarter-wave plate to focus the laser beam at the center of the cross slot. The focal region is approximately cylindrical with a width given by $d_f = (4\lambda/\pi)(f/D)$. Here, λ is the wavelength (633 nm), f = focal length of the lens (100 mm), and D = diameter of the laser beam at half-width (1.3 mm). The depth of focus, l_f, of the focal cylinder is approximately $l_f = (8\lambda/\pi)(f/D)^2$.[25] By translating the lens and maintaining l_f close to the path length in the neutral direction (10 mm), we produced $d_f \sim 60\ \mu$m. This value, small compared to the 500 μm dimension of the cross-slot, determines the spatial resolution of the birefringence apparatus. The flow cell was mounted on a two-dimensional micropositioning stage and translated with resolution of 5 μm to conduct spatially resolved birefringence studies along the inlet and outlet axes of the flow. The data are reported in Figure 3 for a nominal strain rate of $1.92 \times 10^4\ s^{-1}$ in flow device FC-2. The weight-average molar mass and concentration of the PEO solution are 4.7×10^6 g/mol and 500 ppm, respectively. As reported in Figure 3, birefringence along the inlet axis is small except in the center of the device. Enhanced birefringence persists along the outlet axis far from the cross-slot center. These results are consistent with previous measurements of the birefringence in stagnation point flows,[1,30] thereby estab-

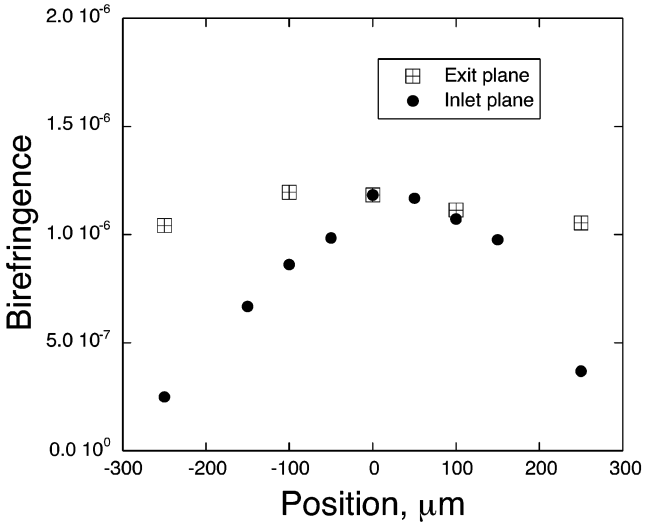

Figure 3. Birefringence intensity at the inlet and exit planes as a function of distance from the center of the cross-slot. The sample PEO5M at 500 ppm was subjected to a strain rate, $\dot{\epsilon}$, of 1.92×10^4 s^{-1}.

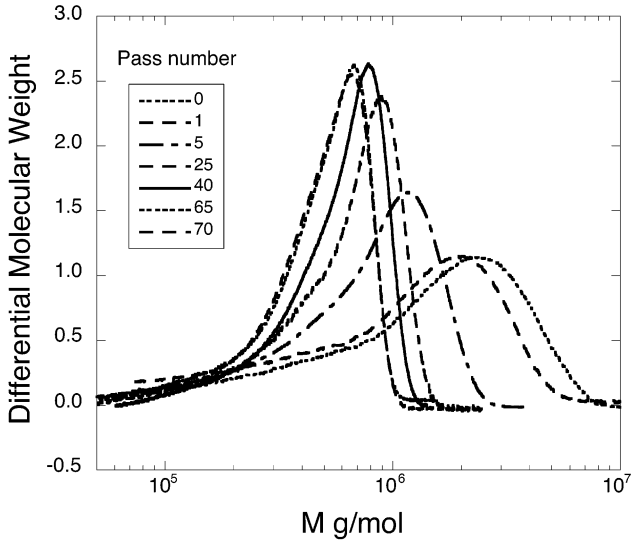

Figure 4. Molecular weight distribution (MWD) obtained for PEO5M/water sample after the 200 ppm solution was passed through the flow cell FC-1 at $\dot{\epsilon} = 2.42 \times 10^4$ s^{-1} for different number of passes. The MWD shifts toward lower molecular weight with increasing number of passes.

lishing the correspondence between the devices used here and previous experiments reported in the literature.

C. Gel Permeation Chromatography. The molar mass distribution of PEO was measured by means of gel permeation chromatography (GPC, Waters Corp., Milford, MA) with refractive index and multiangle laser light scattering (MALLS) detection. Degassed and filtered 0.1 M $NaNO_3$ aqueous buffer was pumped (Waters 515) at an elution rate of 0.2 mL/min through two temperature-controlled ($T = 50$ °C) columns (PL-aquagel-OH 50 and PL-aquagel-OH 60, Polymer Laboratories Inc., Amherst, MA). Filtered (1.0 μm pore size) samples (250 μL) were injected by means of an autosampler (Waters 717 Plus). The concentrations of separation products were determined by a refractive index detector (Optilab DSP, Wyatt Corp., Santa Barbara, CA).

The radius of gyration (R_g) and molar mass of separated fractions were assessed by means of static light scattering (Dawn EOS, Wyatt Corp., Santa Barbara, CA) of eluted fractions and application of the Berry formalism, under the assumption of the osmotic second virial coefficient (A_2) equal to zero. Because of the low concentration of eluted fractions, independent assessment of A_2 by batch mode static light scattering indicates that the assumption of $A_2 = 0$ yields an error in the characterization of molar mass of no greater than 0.5%. The number-average (M_n) and weight-average (M_w) molar mass were determined by computing moments of the measured molar mass distribution. The performance of the GPC and MALLS system for characterization of poly(ethylene oxide) (PEO) molar mass was determined by measuring the molar mass of standards of $M_w = 2.19 \times 10^5$ g/mol and 9.20×10^5 g/mol (see Table 1). The relative error for each determination was 1.3% and 0.8%, respectively.

III. Results

A. Scission Molar Mass Distribution. Test solutions were cycled at dilute concentrations through the cross-slot device multiple times to achieve a steady-state scission product molar mass distribution. The molar mass distribution as a function of pass number for a 200 ppm PEO solution at nominal strain rate $\dot{\epsilon} = 24\,200$ s^{-1} tested in flow cell FC-1 is plotted in Figure 4. Progressive degradation of the polymer occurs until a steady state is achieved at 65−75 passes. The large number of passes arises because molecules traversing different streamlines in the stagnation region of the cross-slot flow experience different probabilities of breakage. Thus, overall, the scission probability for any molecule passing through the device is low, and test solutions must be passed through the device multiple times to achieve a steady-state molar mass distribution.

We estimated the probability that a chain is broken in the flow on a per pass basis by means of a simple model. The model assumes that chains with molar mass greater than the steady-state weight-average molar mass, $M_{w,f}(\dot{\epsilon})$, undergo midpoint scission with a probability that is a constant for all passes. If each pass is treated independently, the best fit to data such as in Figure 4 indicates that this probability is typically 15−20% of chains broken per pass.

To evaluate the extent to which the scission experiments (e.g., Figure 4) were conducted in the dilute regime, we compared per pass evolution of the molar mass averages for PEO solutions with concentrations 200 ppm ($c/c^* = 0.065$) and 20 ppm ($c/c^* = 0.0065$). Here, we take the overlap concentration, $c^* \approx 3M/4\pi R_g{}^3 N_A = 3075$ ppm where M and R_g are characteristic molar mass and radius of gyration, respectively, and N_A is Avogadro's number. Results are reported in Figure 5. Although intermolecular interactions and flow modifications are reported at concentrations well below the overlap concentration,[2,3] in this case the scission molar mass distributions for the two concentrations are not distinguishable. Consequently, all studies were conducted at 200 ppm.

B. Effect of Upstream Contraction. The qualitative effect of an upstream contraction on the scission product molar mass distribution of 200 ppm aqueous PEO solutions in cross-slot flow is reported in Figure 6a,b. For these independent experiments, the cross-slot flow devices were operated in two modes. The first mode, with two inlets and two outlets, generates a stagnation point flow in the cross-slot after the flow experiences an upstream contraction and before the flow experiences a downstream expansion. The second mode, with only one inlet and one outlet, does not generate a stagnation flow but still realizes the upstream contraction as well as the downstream expansion. The second mode assesses the capacity of the upstream contraction to directly generate chain scission. The difference between

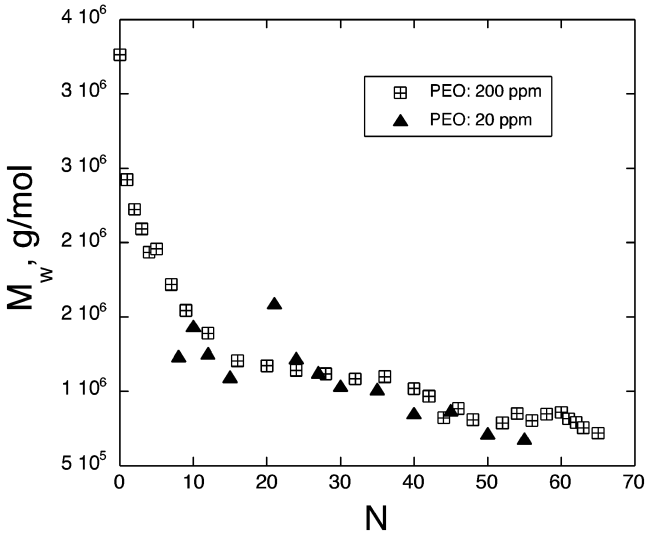

Figure 5. Average molecular weight of PEO5M/water polymer solutions against number of passes through the flow cell FC-1. Similar strain rates ($\dot{\epsilon} \sim 12 \times 10^3\ s^{-1}$) were used at two different concentrations: 20 ppm (triangle) and 200 ppm (square).

the two data sets characterizes the additional effect of the stagnation point flow on chain scission. Figure 6a shows that at comparable average velocities the stagnation flow and contraction flow combination breaks chains in a significantly more efficient manner than the contraction flow alone. That is, although chains are broken by the upstream contraction, the steady-state molar mass of scission products is ultimately determined by scission in the cross-slot device since the contraction-stagnation curve lies below the contraction-only curve in Figure 6a.

Comparison of the data from the flow devices with abrupt (Figure 6a) and tapered (Figure 6b) upstream contractions demonstrates that the steady-state molar mass of the scission products in the cross-slot flow is not a function of the detailed geometry of the upstream contraction, since the relative difference between the molar mass yielded in the two devices is small for comparable average velocities. Thus, the steady-state molar mass of scission products extracted from data like Figures 5 and 6 is dominated by the effect of the planar stagnation flow field rather than the upstream contraction that is also necessarily present. This result is one principal finding of our study.

C. Effect of Reynolds Number on the Strain Rate Scaling of the Steady-State Molar Mass Distribution. Sections IIIA and IIIB argue that the steady-state molar mass of scission products resulting from planar elongational flow can be extracted from multipass flow studies in the two available flow cell devices. By means of this procedure, scission experiments were conducted at a range of nominal strain rates to extract the scaling of the critical molar mass ($M_{w,f}$) for fracture with strain rate ($\dot{\epsilon}$). This scaling is a principal prediction of theories of flow-induced polymer chain scission.[9,12,14] Figure 7 reports typical results for aqueous PEO solutions at three nominal strain rates in cross-slot flow device FC-1 from which the steady-state scission molar mass was determined. Qualitatively, Figure 7 demonstrates that increasing nominal strain rate yields a decrease in critical molar mass.

Figure 8 summarizes the results of experiments with 200 ppm PEO solutions over a range of nominal applied

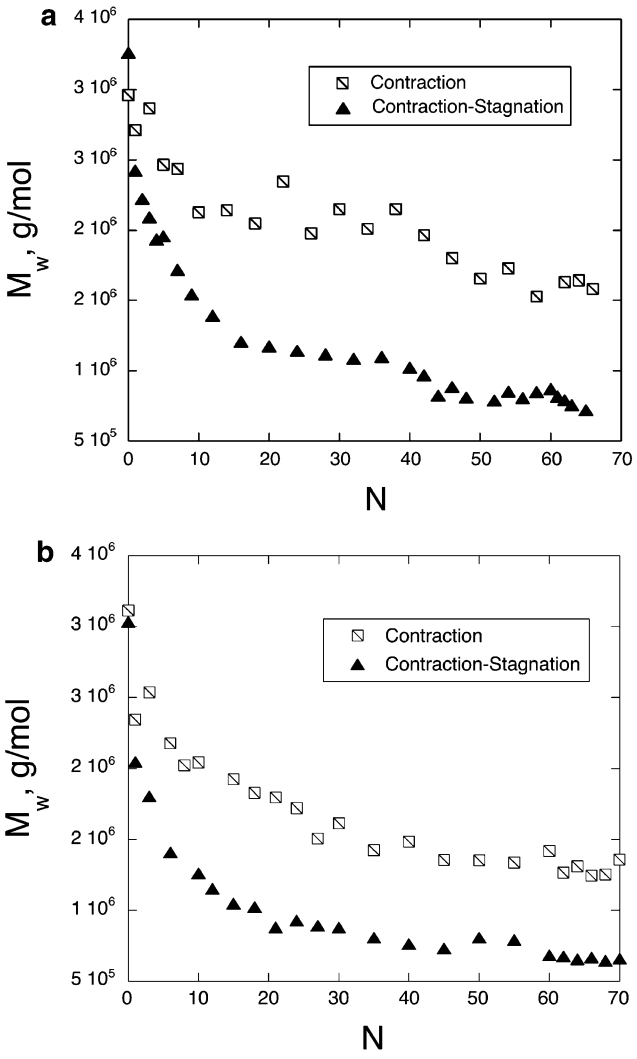

Figure 6. (a) Average molar mass for PEO5M/water (concentration 200 ppm) against number of passes for contraction-only (squares) and contraction-stagnation point (triangles) flows through the flow cell with abrupt upstream contraction (FC-1). To maintain similar average strain rates in the two cases, the flow rate during contraction-only experiments (1.80 L/min) was set at approximately half the flow rate of the contraction-stagnation case (3.16 L/min). (b) Average molar mass for PEO5M/water (concentration 200 ppm) against number of passes for contraction-only (squares) and contraction-stagnation point (triangles) flows through the flow cell with gradual upstream contraction (FC-2). To maintain similar average strain rates in the two cases, the flow rate during contraction-only experiments (1.35 L/min) was set at approximately half the flow rate of the contraction-stagnation case (2.51 L/min).

strain rates. Data are for experiments in both flow devices as well as from PEO solutions that were initially either polydisperse or monodisperse. In aqueous solutions and at high Re, we find the scaling $\dot{\epsilon} \propto M_{w,f}^{-1.04\pm0.07}$. This scaling exponent was assessed over the accessible strain rate range of $3600\ s^{-1} < \dot{\epsilon} < 26\,400\ s^{-1}$. This range corresponds to $910 < Re < 6600$. The range of molar masses over which these experiments were characterized spans more than 1 decade.

The effect of Reynolds number on the strain rate scaling of the critical molar mass for chain scission was assessed by means of experiments in a 50:50 aqueous glycerol mixture with $\mu = 6.4$ mPa s. For this solvent, the studied strain rate range is $1700\ s^{-1} < \dot{\epsilon} < 24\,000\ s^{-1}$, corresponding to $70 < Re < 940$. As reported in

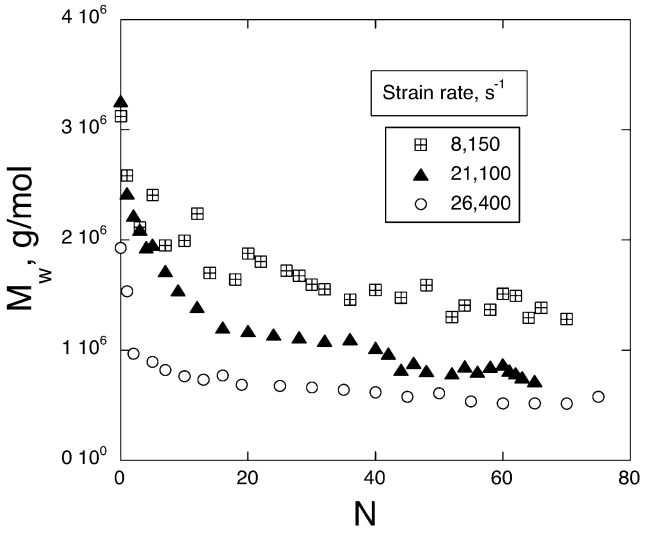

Figure 7. Average molar mass against number of passes for PEO5M (200 ppm concentration) solutions in water for different strain rates.

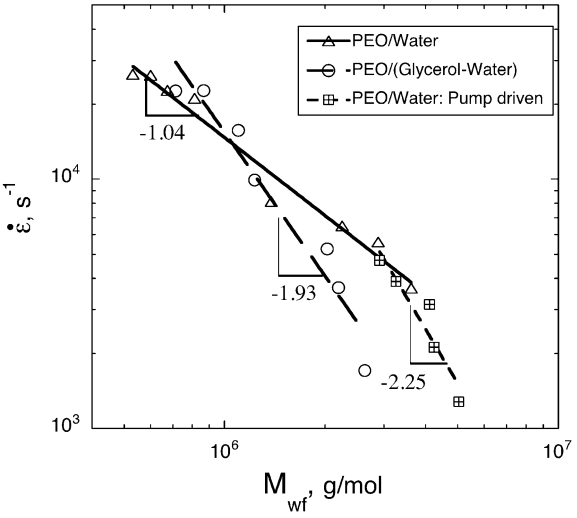

Figure 8. Imposed strain rates are plotted against critical molecular weight for chain fracture for PEO. The triangles are for experiments with aqueous PEO solutions performed using the pressure driven flow apparatus and the squares are from experiments carried out in the pump driven flow loop. The circles are for the viscous solvent (water/glycerol: 50/50; $\eta_0 =$ 6.4 cP) passed through the flow cell in a pressure-driven configuration.

Figure 8, in this interval we find a strikingly different dependence of critical scission molar mass on nominal strain rate: $\dot{\epsilon} \propto M_{w,f}^{-1.93 \pm 0.15}$.

Scission experiments with aqueous solutions were also performed at low Re with the pump-driven flow apparatus. The scaling exponent obtained in this case was $\dot{\epsilon} \propto M_{w,f}^{-2.25 \pm 0.10}$ for the strain rate range of 1280 $s^{-1} < \dot{\epsilon} < 4730\ s^{-1}$ corresponding to $320 < Re < 1180$.

In the above discussion, we define the Reynolds number, $Re = \rho Q/\mu l$, to be consistent with the usual definition of strain rate in the scission literature (cf. section IIB). Here ρ is the fluid density, Q is the total volumetric flow entering the device through the two inlets, l is the slot height, and μ is the solvent viscosity. However, note that this definition differs by a factor of 2 from the definition used in previous fluid dynamics studies of stagnation point flows.[32]

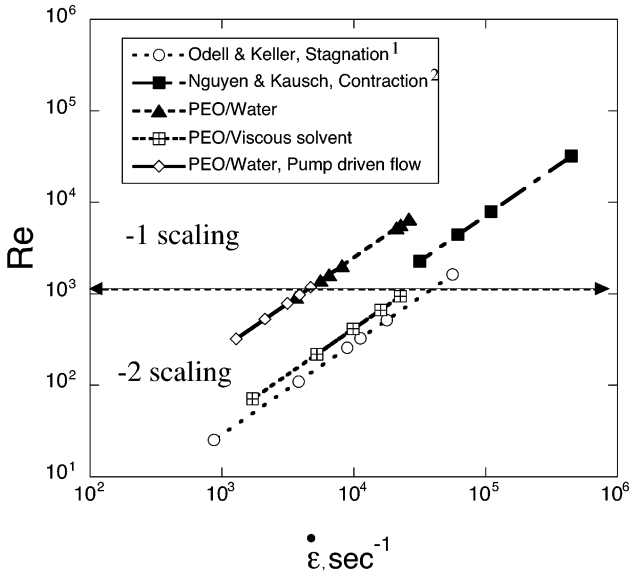

Figure 9. Flow regimes for polymer chain scission experiments performed for PEO and polystyrene (literature data) samples using different flow geometries. Results presented in Figure 8 are plotted along with the literature data. Filled symbols represent results in which a scission scaling exponent of ~ -1 has been reported. Open symbols display findings in which a scaling of ~ -2 has been assigned.

IV. Discussion

This study has discovered that differences in polymer chain scission exponents previously attributed to different molecular mechanisms for scission are equally well explained as an effect induced by differences in the Reynolds number at which the experiments were performed. In this section, we review the results from this study that support this conclusion. As an additional test, we revisit literature data in the context of Reynolds number effects and find that prior results are consistent with our hypothesis. Finally, we report measurements of the pressure drop that further characterize the role of inertia in flow field modification in cross-slot flow.

The literature has suggested that $\dot{\epsilon}_f \sim M^{-2}$ when polymer molecules break according to a quasi-steady-state mechanism, as in planar elongational flow,[1] and $\dot{\epsilon}_f \sim M^{-1}$ when molecules break according to a fast transient scission mechanism, as in flow through an abrupt contraction.[2,9] Figure 8 suggests that the transition between these two scission scaling regimes is controlled by Reynolds number, since increasing the solution viscosity or decreasing the characteristic flow rate causes the scission of PEO molecules to transform from a process with scaling ~ -1 to a process with scaling ~ -2. The difference in scaling exponents quantified is certainly statistically significant: the range of polymer molar masses probed is greater than a decade, and the standard deviation in the exponent is less than ± 0.15 in all cases.

The role of inertial effects in mediating the scaling of the critical scission molar mass is made more apparent by plotting the experimental data vs the Reynolds number of the flow in the cross-slot, as reported in Figure 9. The data fall onto two curves, corresponding to experiments in the aqueous solution and in the viscous glycerol water mixture. To assess the consistency of our data with previous literature results, we also replot measurements of refs 1 and 2. For results in which a scission exponent of ~ -1 was reported, we

represent the data with filled symbols. We use open symbols for data for which a scission exponent of ~ -2 has been assigned. To our knowledge, this plot displays all the data from which critical scission scaling exponents have been extracted in the past.

When plotted in this way, the origin of the distinction between data sets is strikingly apparent. The transition between the two scaling regimes of the data sets occurs at Re $\sim$ 1000. Figure 9 is our central result. It demonstrates that measurements from three different studies are all consistent with an effect of flow inertial character on chain scission exponents. Since Figure 9 results encompass a range of polymer/solvent systems, we conclude that the Re number transition reported here is likely a universal feature of scission that is independent of chain architecture and solvent quality.

We searched for direct evidence of such an inertial transition by means of pressure drop measurements in the cross-slot device. The following study was conducted: Pressure taps (Cole-Parmer, Vernon Hills, IL) were installed in the flow cell with a gradual contraction (FC-2). Measurements were performed at a range of flow rates using the solvent systems previously devised for chain scission experiments. The measurements were made in two different configurations. The first was the configuration of the previously reported chain scission experiments. In this case, one pressure transducer was placed at the inlet before the upstream contraction and the other one at the outlet after the downstream expansion. The pressure drop thus measured is the sum of the contributions from the upstream contraction, stagnation region, and downstream expansion of the flow. In the second configuration, two opposite ends of FC-2 were closed, and the solvents flowed from the inlet through the upstream contraction into the outlet via the downstream expansion. This configuration does not generate a stagnation point flow and therefore assesses the contribution of the upstream contraction and downstream expansion to the total pressure drop measured in the first mode.

Figure 10a reports measurements from the two different configurations for the viscous solvent consisting of 50/50 water/glycerol. Measurements above and below Re $\sim$ 1000 were conducted because of the suggested relevance of this range as per Figure 9. A discontinuity in the slope of the pressure drop vs Reynolds number curve is apparent at Re $= 860 \pm 30$ when the stagnation point flow is operational. This discontinuity is not present in the second configuration that probes only contraction and expansion effects. Thus, this transition, at Re about 1000, is associated with the stagnation point region of flow device FC-2. Figure 10b investigates if the transition occurs in a solvent of different viscosity. In water, a discontinuity in the pressure drop vs Re curve occurs at Re $= 1240 \pm 55$. Figure 10a,b directly confirms the presence of an inertia driven flow transition at Re $\sim$ 1000, as suggested indirectly by the scission data of Figure 9. Muller et al.'s[33] reported flow transition at Re $\sim$ 850 in flow through opposed jets also indirectly supports our hypothesis of inertial transition in stagnation point flows at Re $\sim$ 1000.

It is of interest to assess other implications of this newly discovered Re number transition for flow-induced polymer scission. For example, we find that scission products of nearly monodisperse and polydisperse polymer samples display unimodal scission distributions for Re > 1000 (cf. Figure 4) that are inconsistent with the

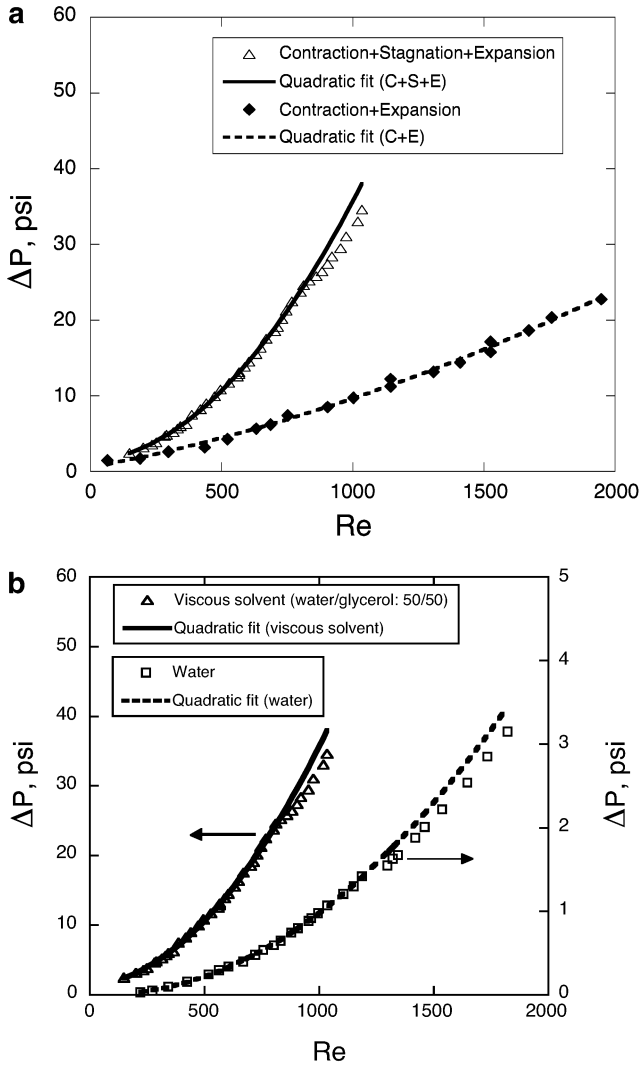

Figure 10. (a) Pressure drop at different configurations for the flow of glycerol−water (50:50) test fluid through FC-2. The solid line is a quadratic fit to the data at low Reynolds numbers for the stagnation point arrangement. The change of curvature of data points at high Re (Re > 860) is indicative of an inertial flow transition. The contraction−expansion configuration does not exhibit similar deviation from the quadratic fit. (b) Pressure drop in stagnation point flow configuration for two solvents of different viscosity. The lines are a quadratic fit through the data points at low Re. Discontinuities in the slopes of the experimental curves at high Re quantify inertially driven flow transitions.

midpoint scission hypothesis that has been apparently well corroborated in the literature under other conditions.[1,2,4,16,17] It is remarkable that fluid inertia, a continuum fluid dynamical quantity, can affect details of the molecular process of scission to this degree, and thus further studies of such effects on the scission molar mass distribution are warranted.

In conclusion, experiments designed to directly test molecular mechanisms of polymer chain scission must be conducted at Reynolds numbers lower than have been performed to date. Since inertial effects significantly affect scaling relationships that previously have been taken as evidence for a particular scission mechanism, the effect of Reynolds number on other measures of polymer chain scission should be evaluated. In addition, the mechanism by which inertially modified flow affects the molecular level process of polymer chain scission should be further investigated.

Acknowledgment. We thank Amy Herzog for intrinsic viscosity measurements, Ramana Vishnubhotla for help with experiments, Joe LaCour for help with figure schematics, and Prof. Ronald Larson, Prof. Wesley Burghardt, and Mr. Chih-Chen Hsieh for valuable discussions. This research was supported by DARPA under Contract MDA972-01-1-0020.

References and Notes

(1) Odell, J. A.; Keller, A. *J. Polym. Sci., Polym. Phys. Ed.* **1986**, *24*, 1889.
(2) Nguyen, T. Q.; Kausch, H. H. *Adv. Polym. Sci.* **1992**, *100*, 73.
(3) Keller, A.; Odell, J. A. *Colloid Polym. Sci.* **1985**, *263*, 181.
(4) Horn, A. F.; Merrill, E. W. *Nature (London)* **1984**, *312*, 140.
(5) Hunston, D. L.; Zakin, J. L. *Polym. Eng. Sci.* **1980**, *20*, 517.
(6) Merrill, E. W.; Leopairat, P. *Polym. Eng. Sci.* **1980**, *20*, 505.
(7) Nguyen, T. Q.; Kausch, H. H. *Chimia* **1986**, *40*, 129.
(8) Kim, C. A.; Kim, J. T.; Lee, K.; Choi, H. J.; Jhon, M. S. *Polymer* **2000**, *41*, 7611.
(9) Nguyen, T. Q.; Porouchani, R.; Kausch, H. H. In *Flexible Polymer Chains in Elongational Flow: Theory and Experiment*; Nguyen, T. Q., Kausch, H. H., Eds.; Springer-Verlag: Berlin, 1999.
(10) Narh, K. A.; Odell, J. A.; Muller, A. J.; Keller, A. *Polym. Commun.* **1990**, *31*, 2.
(11) Choi, H. J.; Lim, S. T.; Lai P. Y.; Chan, C. K. *Phys. Rev. Lett.* **2002**, *89*, 088302.
(12) Ryskin, G. *J. Fluid Mech.* **1987**, *178*, 423.
(13) Rabin, Y. J. *J. Chem. Phys.*, **1987**, *86*, 5215.
(14) Rabin, Y. *J. Non-Newtonian Fluid Mech.* **1988**, *30*, 119.
(15) Nguyen, T. Q.; Kausch, H. H. *J. Non-Newtonian Fluid Mech.* **1988**, *30*, 125.
(16) Lim, S. T.; Choi, H. J.; Lee; S. Y.; So, J. S.; Chan, C. K. *Macromolecules* **2003**, *36*, 5348.
(17) Odell, J. A.; Taylor, M. A. *Biopolymers* **1994**, *34*, 1483.
(18) Scrivener, O.; Berner, C.; Cressely, R.; Hocquart, R.; Sellin, R.; Vlachos, N. S. *J. Non-Newtonian Fluid Mech.* **1979**, *5*, 475.
(19) Hunkeler, D.; Nguyen, T. Q.; Kausch, H. H. *Polymer* **1996**, *37*, 4257.
(20) Odell, J. A.; Muller, A. J.; Narh, K. A.; Keller, A. *Macromolecules* **1990**, *23*, 3092.
(21) Hur, J. S.; Shaqfeh, E. S. G.; Babcock, H. P.; Chu, S. *Phys. Rev. E* **2002**, *66*, 011915.
(22) Reese, H. R.; Zimm, B. H. *J. Chem. Phys.* **1990**, *92*, 2650.
(23) Odell, J. A.; Carrington, S. P. In *Flexible Polymer Chains in Elongational Flow: Theory and Experiment*; Nguyen, T. Q., Kausch, H. H., Eds.; Springer-Verlag: Berlin, 1999.
(24) Nguyen, T. Q.; Kausch, H. H. *Macromolecules* **1990**, *23*, 5137.
(25) Nguyen, T. Q.; Yu, G.; Kausch, H. H. *Macromolecules* **1995**, *28*, 4851.
(26) Dontula, P.; Macosko, C. W.; Scriven, L. E. *AIChE J.* **1998**, *44*, 1247.
(27) Miles, M. J.; Keller, A. *Polymer* **1980**, *21*, 1295.
(28) Odell, J. A.; Keller, A.; Rabin, Y. *J. Chem. Phys.* **1988**, *88*, 4022.
(29) Larson, R. G. *J. Non-Newtonian Fluid. Mech.* **2000**, *94*, 37.
(30) Carrington, S. P.; Tatham, J. P.; Odell, J. A.; Saez, A. E. *Polymer* **1997**, *38*, 4151.
(31) Fuller, G. G. *Optical Rheometry of Complex Fluids*; Oxford University Press: New York, 1995.
(32) Lagnado, R. R.; Leal, L. G. *Exp. Fluid.* **1990**, *9*, 25.
(33) Muller, A. J.; Saez, A. E.; Odell, J. A. *AIChE J.* **1995**, *41*, 1333.

MA035254U